Solar Energy Materials & Solar Cells 252 (2023) 112180

Contents lists available at ScienceDirect

Solar Energy Materials and Solar Cells

journal homepage: www.elsevier.com/locate/solmat

Reducing sputter damage-induced recombination losses during deposition of the transparent front-electrode for monolithic perovskite/silicon tandem solar cells

Marlene Härtel [a,b], Bor Li [b], Silvia Mariotti [b,1], Philipp Wagner [b], Florian Ruske [c], Steve Albrecht [a,b,*], Bernd Szyszka [a,d,**]

[a] Technische Universität Berlin, Fakultät Elektrotechnik und Informatik, Marchstraße 23, 10587, Berlin, Germany
[b] Perovskite Tandem Solar Cells, Helmholtz-Zentrum Berlin, Kekuléstraße 5, 12489, Berlin, Germany
[c] Active Materials and Interfaces for Stable Perovskite Solar Cells, Helmholtz-Zentrum Berlin, Kekuléstraße 5, 12489, Berlin, Germany
[d] PVcomB, Helmholtz Zentrum Berlin, Schwarzschildstr. 3, 12489, Berlin, Germany

ARTICLE INFO

Keywords:
Sputter damage
Perovskite/silicon tandems
Tandems
Transparent conductive oxides
Non-radiative recombination losses
Optical simulation

ABSTRACT

Many research groups work on overcoming the 30% power conversion efficiency (PCE) level for perovskite/silicon tandem solar cells with various approaches. The most common tandem architectures employ a transparent conductive oxide (TCO) front electrode. Due to its fast deposition and up-scalability, sputter deposition is the preferred method for TCO deposition. The sensitive layers of perovskite solar cells are protected from sputter damage by a thermal atomic layer (ALD) deposited tin oxide (SnO_2) buffer layer, which induces parasitic absorption. Here, we propose a method to reveal the impact of sputter damage on SnO_2 buffer layer-free devices. By performing light intensity-dependent current density-voltage (J-V) measurements and thereby reconstructing the single-junction solar cell pseudo J-V characteristics, we could associate sputter damage with trap-assisted non-radiative recombination losses. Additionally, we demonstrate a simple method to minimize sputter damage to the perovskite solar cell to the point where a protective SnO_2 buffer layer is no longer required. By lowering the sputter power density during the TCO deposition, we regained ~13 mV open-circuit voltage and ~3% fill factor of the devices, improving the efficiency from 13.55 to 14.17%. We show that these improvements are linked to a reduction of transport and non-radiative recombination losses. Finally, we fabricated optically superior and sputter damage-free monolithic perovskite/silicon tandem devices without needing a protective SnO_2 buffer layer. By doing so, we increased the tandem device current density by 0.52 mA/cm^2, representing a crucial step toward further optimizing the optical performance of tandem devices.

1. Introduction

Due to their high efficiency potential of over 30%, perovskite/silicon tandem solar cells have captivated the attention of scientific and industrial research and development [1]. A monolithically integrated tandem device currently holds the current world record power conversion efficiency (PCE) for perovskite/silicon tandem solar cells, at 29.8% [2]. The efficient conversion of light to electrical energy over a wide wavelength range without high losses from thermalization accounts for its outstanding efficiency [1]. The tandem top-cell consists of a perovskite absorber with a wide band gap (1.68 eV), and the silicon bottom-cell has a low band gap (1.12 eV). A highly transparent conductive oxide (TCO) front-electrode, meaning a high optical band gap, low free charge carrier absorption, and sufficient thickness to assure a low enough series resistance that does not reduce the fill factor, is required in order to minimize optical losses. Sputtering is the method of choice to deposit TCOs as it is known to be capable of producing high-quality films and it is easy to scale up to mass production

* Corresponding author. Technische Universität Berlin – Fakultät Elektrotechnik und Informatik, Marchstraße 23, 10587, Berlin.
** Corresponding author. Technische Universität Berlin – Fakultät Elektrotechnik und Informatik, Marchstraße 23, 10587, Berlin.
E-mail addresses: m.haertel@tu-berlin.de (M. Härtel), bor.li@helmholtz-berlin.de (B. Li), silvia.mariotti@oist.jp (S. Mariotti), philipp.wagner@helmholtz-berlin.de (P. Wagner), florian.ruske@helmholtz-berlin.de (F. Ruske), steve.albrecht@helmholtz-berlin.de (S. Albrecht), bernd.szyszka@tu-berlin.de (B. Szyszka).
[1] Now at Energy Material and Surface Sciences Unit, Okinawa Institute for Science and Technology Graduate University (OIST), 1919-1, Tancha, Onna Son, Okinawa, 904-0495, Japan

https://doi.org/10.1016/j.solmat.2023.112180
Received 1 July 2022; Received in revised form 14 October 2022; Accepted 2 January 2023
Available online 11 January 2023

environments [3–5]. However, sputtering is known to induce sputter damage to sensitive substrates [4,6–11]. Demaurex et al. observed damage on the hydrogenated amorphous/crystalline silicon interface passivation when sputter depositing indium tin oxide (ITO) in a reactive direct current (DC) process, while they partly assigned the carrier lifetime reduction to UV irradiation during the plasma deposition process [10]. Werner et al. deposited indium zinc oxide (IZO) from a ceramic target in a radio frequency (RF) magnetron sputter process onto the organic hole transport layer (HTL) Spiro-MeOTAD [4]. They observed s-shapes in the J-V characteristics reducing the fill factor (FF) and the efficiency. By applying light intensity-dependent J-V measurements following Tress and colleagues [12], they could identify that the sputter damage resulted in an extraction barrier, which was dependent on the applied sputter power. Likewise, Kanda et al. observed an s-shaped J-V characteristic for their perovskite solar cells after depositing ITO on Spiro-MeOTAD in an RF sputter process [13]. Their model approach revealed a Schottky barrier in the HTL/TCO interface that is dependent on the sputtering time. Sputter damage for the p-i-n (so-called "inverted") perovskite solar cell designs was observed by Wahl et al. [7]. In a DC sputter process, they deposited IZO electrodes on the electron transport layer (ETL). The damage also leads to s-shaped J-V curves originating from a disorder of the organic ETL in the interface, which a short annealing step could cure. Recently, Liu et al. presented their results on sputter damage in perovskite/silicon tandem solar cells [11]. They deposited IZO in an RF sputtering process onto either bathocuproine (BCP) or SnO_2 in order to compare the impact of sputter damage and stress on the underlying films. Furthermore, they varied the target to substrate distance. According to their results, a SnO_2 buffer layer is necessary to protect against sputter damage. Their simulation showed that sputtered atoms with energies of as low as 6 eV could break C–C bonds in the BCP. However, during cathode sputtering, kinetic energies of sputtered species range between a few eV and up to several hundred eVs. Among them, oxygen ions (O^-) and reflected neutrals were found to have the highest kinetic energy, reaching values as high as the target discharge voltage (eV_t), which are still detectable at the substrate [8,14]. Several groups have looked into ways to reduce the impact of the kinetic energy of the O^- species by either tuning the target discharge voltage [14], by performing an indirect deposition where only scattered particles reach the substrate [15], or by sputtering through a negatively biased mesh electrode, thereby repelling the O^- species [6]. The target discharge voltage is dependent on several factors, such as the applied sputter power, the process pressure, the target's conductivity, the magnetic field strength at the target surface, or the discharge mode. The target discharge voltage is commonly higher for DC processes compared to RF processes. However, we observed a target voltage as high as 200 V for our highest RF sputter power, leading to high and possibly damaging kinetic particle energies.

In this work, we propose a method to reveal and correlate the actual impact of sputter damage on the perovskite solar cell performance with recombination dynamics in the device by performing light intensity-dependent J-V measurements to reveal sputter damage-induced losses. To the best of our knowledge, this approach in this context is unprecedented. Furthermore, we show that reducing the sputter power, a simple modification of the sputter process, is sufficient to reduce sputter damage-induced transport and non-radiative recombination losses, improving the solar cell performance. We simultaneously assure optically and electrically equal IZO films. This approach was tested on perovskite solar cells by directly sputtering on the sensitive electron charge transport layer without a protective SnO_2 buffer layer. We refer to the approach as soft sputtering. Finally, we discuss the applicability of SnO_2 buffer layer free perovskite top-cell in the monolithic tandem configuration and show the optical superiority of this approach over the conventional design.

2. Experimental

2.1. Sample preparation

For optical and electrical analysis of the TCO, 100 nm thick IZO layers were sputter deposited via RF magnetron sputtering in a Roth-&Rau MicroSys 200 PVD system on quartz glass substrates. The target used had a size of 2 inches and a composition of 90 wt% In_2O_3 and 10 wt % ZnO (purchased from FHR Anlagenbau GmbH). Two RF power densities were investigated, 4.21 W/cm^2 and 2.41 W/cm^2. Both processes were dynamic, meaning the substrate oscillates at a 30° angle below the target surface at a distance of approximately 17 cm. The process pressure was 6 x 10^{-3} mbar, and the base pressure prior to the sputter deposition was 10^{-7} mbar. The argon/oxygen gas flow in each case was in sum 40 sccm. The first process had a total of 0.25% oxygen mixed in, and the second had 0.1% oxygen mixed in. We optimized these values by performing an oxygen series test for both power densities prior to the experiments in order to find an argon/oxygen gas flow ratio for the low power process, that yields optically and electrically equivalent IZO films.

The discussed semitransparent perovskite single-junction solar cells were in inverted structure (p-i-n), with the following design: commercial laser-patterned ITO coated glass substrates/2-PACz/perovskite/LiF/C_{60}/PEIE/IZO/Ag fingers. The Ag fingers are located outside the active area and shorten the charge transport path over the IZO. The ITO-coated glass substrates (25 × 25 mm, 15 Ω/sq, laser-patterned by Automatic Research GmbH) were cleaned in Mucasol (2%$_{vol}$ in water, substrate surfaces were rubbed with a glove), DI-water, acetone, and isopropanol subsequently, in an ultrasonic bath. Each step was carried out for 10 min, and after Mucasol, the samples were purged with DI-water. Prior to the 2-PACz ([2-(9*H*-carbazol-9-yl)ethyl]phosphonic acid) spin-coating step, the samples were treated in a UV-ozone cleaner (FHR UVOH 150 Lab) for 15 min. The HTL 2-PACz (TCI) was dissolved in ethanol (1 mmol/l ml solution) and spin-coated (5 s acceleration at 3000 rpm, 15 s duration at 3000 rpm) in a nitrogen atmosphere and annealed for 5 min at 100 °C. The 1.5 M perovskite precursor was prepared in a $FAPbI_3$ to $MAPbBr_3$ volume ratio of 77:23, with 5 vol% of 1.5 M nominal CsI. The precursor components FAI and MABr were purchased from Dyenamo, PbI_2 and $PbBr_2$ from TCI, and CsI from abcr GmbH. The precursor was then dissolved in DMF:DMSO = 4:1 vol and placed in a shaker for 90 min at 60 °C. Subsequently, 100 µl of perovskite solution was spin-coated (5 s acceleration and 35 s duration at 3500 rpm) in a nitrogen atmosphere. After 25 s of the spin-coating process, 300 µl of the anti-solvent Anisole was dropped on the perovskite film. The resulting perovskite absorber has a thickness of ~550 nm and a band gap of 1.68 eV. Following the spin-coating step, the films were annealed at 100 °C for 20 min. The subsequent two layers were done in one vacuum run. 1 nm LiF (Sigma Aldrich) passivation layer was thermally evaporated at a rate of 0.05 Å s^{-1} onto the perovskite film, directly followed by the ETL, 18 nm C_{60} (CreaPhys GmbH) layer at a rate of 0.15 Å s^{-1}. Before IZO sputter deposition, a thin film (≈2 nm) of polyethyleneimine ethoxylated (PEIE) with a concentration of 0.025 wt.-% (original solution in water 37 wt.-% diluted with IPA) was spin-coated (1 s acceleration at 5000 rpm, 15 s duration at 5000 rpm) onto the C_{60}. After the sputter deposition of 100 nm IZO (described above) through a 2-stripes shadow mask, 100 nm Ag was thermally evaporation through a specific mask that only contacts the IZO, without shading the active area, at a rate of 1 Å s^{-1}.

The silicon bottom-cells for the tandem devices were manufactured following a similar fabrication process as described by Cruz et al. [16], if not stated otherwise. The bulk silicon consisted of a 260 µm float zone (FZ) Wafer with a resistivity of ~1–3 Ωcm. The (n)nc-SiO:H layer in-between the 5 nm thick (i)a-Si and the TCO-recombination layer had a thickness of 100 nm. The backside (i)a-Si had a thickness of 5 nm. The front side electrode (recombination layer in a tandem device) was 20 nm of InO:H-based TCO film from newSCOT. The rear side electrode consisted of a 110 nm thick InO:H-based TCO film from newSCOT and 400

nm silver. No grid was used on either side. Instead, the active area had a size of 1.1 cm^2, defined by the silver and TCOs. The bottom cell was backside textured, and the front was polished. Also, no SiO_2 film was deposited on the recombination layer.

The perovskite top-cells for the tandem devices were prepared similarly, if not stated otherwise, as described above and by Al-Ashouri et al. [17]. The silicon bottom cell was blow-cleaned with a nitrogen gun and washed with ethanol. Subsequently, the ITO surface of the bottom cells needs to be treated in a 15 min UV-ozone treatment step before spin-coating the HTL. The HTL used for the tandem device fabrication was Me-4PACz dissolved in ethanol (3 mmol solution), while the perovskite solution preparation is equal to the one described before. The anti-solvent used for tandem devices was ethyl acetate, which results in a thicker perovskite film of ~600 nm. For the devices with tin oxide (SnO_2) buffer, 20 nm SnO_2 was deposited onto the C_{60} via thermal atomic layer deposition (ALD, in an Arradiance GEMStar reactor) instead of PEIE prior to IZO sputter deposition. The Ag frame used to contact the IZO was evaporated through a rectangular-shaped mask around the edges and on top of the IZO electrode, forming the active area of 1 cm^2. Subsequently, 100 nm of LiF anti-reflective coating was thermally evaporated.

2.2. Characterization

The device and sample characterizations were done by current density–voltage (J-V), EQE, spectrophotometry, profilometry, and Hall-effect measurements. Current density-voltage measurements were done on a Wavelabs LED-based Sinus 70 sun simulator (class AAA) at 25 °C, a scan rate of 0.25 V/s and a voltage step-size of 0.02 V. The spectrum was corrected with a non-altered calibrated silicon reference cell prior to the measurement. For the semitransparent single-junction solar cells, a sample holder with a hole was used J-V measurement that enables measurements from both sides by turning the holder around. Back-reflection from surfaces behind the holder was not intentionally suppressed. The single-junctions EQE was measured with a QE-R apparatus from Enlitech. Tandem device EQE was measured by an in-house designed setup. A small illumination spot (2×5 mm^2) was directed to the active area of the tandem device. The measurement was carried out as a function of wavelength in a range of 300–1200 nm (in 10 nm steps). By applying a bias light, the sub-cells are measured independently. Thereby, the top cell is measured applying a bias light of 850 nm wavelength and a voltage of 0.6 V, and the bottom cell is measured applying a bias light of 455 nm wavelength and 0.9 V bias voltage. Solar cell device reflection, as well as transmittance and reflectance of the TCO films, were measured with a PerkinElmer Lambda 1050 dual-beam spectrophotometer equipped with an integrating sphere with photomultiplier tube (PMT) and InGaAs detectors. A calibrated front-side mirror was used as a reflection standard for the TCO measurement, and a spectralon was used to calibrate the setup for the device reflection measurements. The reflection of the devices was measured with a small-spot illumination in a wavelength range from 300 nm to 850 nm (for the single-junctions) or to 1200 nm (for the tandems), with a 10 nm step-size. The transmittance and reflectance of the TCO films were measured from 250 nm to 2500 nm in 5 nm steps. The thickness of the IZO thin films was evaluated by profilometry (DektakXT, Bruker). Electrical characterization of the IZO thin films was done by Hall-effect measurements in van der Pauw geometry (HMS-3000, Ecopia). Ellipsometric spectra were recorded with a Sentech SE850 DUV variable angle spectroscopic ellipsometer. Optical spectra were fitted using the software RIG-VM [18]. Detailed explanations can be found in the supplementary, including recorded and fitted spectra (Figs. S1–4). Optical simulations were conducted using the MATLAB-based program GenPro4 [19].

3. Results and discussion

We designed a TCO sputter deposition process, which aims at minimizing sputter damage to the sensitive (organic) layers of the perovskite solar cell. The flux and energy of highly energetic O^- ions are considered to be directly dependent on the applied power [14]. Therefore, we reduced the RF sputter power density from 4.21 W/cm^2 to 2.41 W/cm^2. The reduction in applied RF power leads to a reduction of the target bias voltage (V_t) from ~200 V to ~140 V. We expect that the reduced target bias voltage leads to lower kinetic energies of the damaging ions during the sputter deposition [4,14]. A schematic illustration of the two different sputter deposition approaches is displayed in Fig. 1a. As the IZO film quality and properties may also impact the photovoltaic parameters of the semitransparent single-junction solar cells, we optimized the deposition process prior to the solar cell application. Therefore, the oxygen to argon flow ratio $O_2/(Ar + O_2)$ was reduced from 0.25% for the IZO deposition with an RF power density of 4.21 W/cm^2 to 0.1% for the IZO deposition with an RF power density of 2.41 W/cm^2. The direct dependence of the optical and electrical properties of the IZO on the oxygen ratio during sputtering has been shown already by Leenheer et al. [20] and Morales-Masis et al. [21]. The resulting 100 nm thick IZO thin films were electrically (see Table 1 and Table S1) and optically (see Fig. 1b) comparable. We investigated the impact of the reduced power density on the photovoltaic parameters of semitransparent single-junction solar cells, where sputter-deposited IZO acts as the transparent front-electrode. The device architecture and illumination direction are shown as a schematic illustration in Fig. 1c. The solar cell FF and V_{OC} increase with decreasing the RF sputter power density (see Fig. 1d and e), overall improving the efficiency from 13.55 to 14.17%. Despite the similar optical performance of the IZO films on quartz-glass (see Fig. 1b), a slight deviation was observed in the EQE of the solar cells (see Fig. 1f), leading to slightly different current densities. The deviation correlates with a shift in the measured 1-R-spectra of the respective solar cells. We note here that the IZO films on quartz-glass were not co-processed with the IZO front electrodes of the solar cells. The deviation in EQE and reflectance in Fig. 1f is likely a sample-to-sample variation (only one sample of each process was analyzed here).

The average V_{OC} of the investigated semitransparent single-junction solar cells could be increased by ~13 mV (from 1.166 V to 1.179 V) by applying a soft IZO sputter deposition (reducing the RF sputter power), and the average FF was increased from ~71% to ~74% by reducing the RF sputter power. A change in V_{OC} is usually related to a better energy level alignment or reduced recombination processes in solar cell devices. In contrast, a solar cell's fill factor is dependent on charge transport inside the device, including transport over the interfaces and the sheet resistance of the TCO, as well as on recombination processes in the bulk and the interfaces.

In order to reveal the origin of sputter damage-induced losses, we performed light intensity-dependent J-V measurements on the semitransparent single-junction solar cells. Such light intensity-dependent measurements can be used to calculate the devices ideality factor [22,23] and determine the so-called pseudo J-V curves. The pseudo J-V curves display theoretical J-V curves independent of series resistance and transport losses and are only limited by recombination processes [24]. In order to obtain pseudo J-V curves, we plotted the J_{SC} against the V_{OC}, which were obtained under light intensity variation. Furthermore, plotting the obtained V_{OC} over the light intensity in a semilogarithmic scale will reveal a linear trend. From the slope of that trend, we calculated the device's ideality factor. The light intensity was varied from 1% (0.01 suns) to 120% (1.2 suns). The resulting plots are displayed in Fig. 2a and b. Additionally, we calculated the contribution of the different loss mechanisms to the device FF for devices that have had their electrode sputter deposited with a power of 4.21 W/cm^2 and 2.42 W/cm^2, according to a methodology described by Stolterfoht et al. [25]. Therefore, we compare the device electrical FF to the pseudo FF obtained from the pseudo J-V curve and the detailed balance limit of a

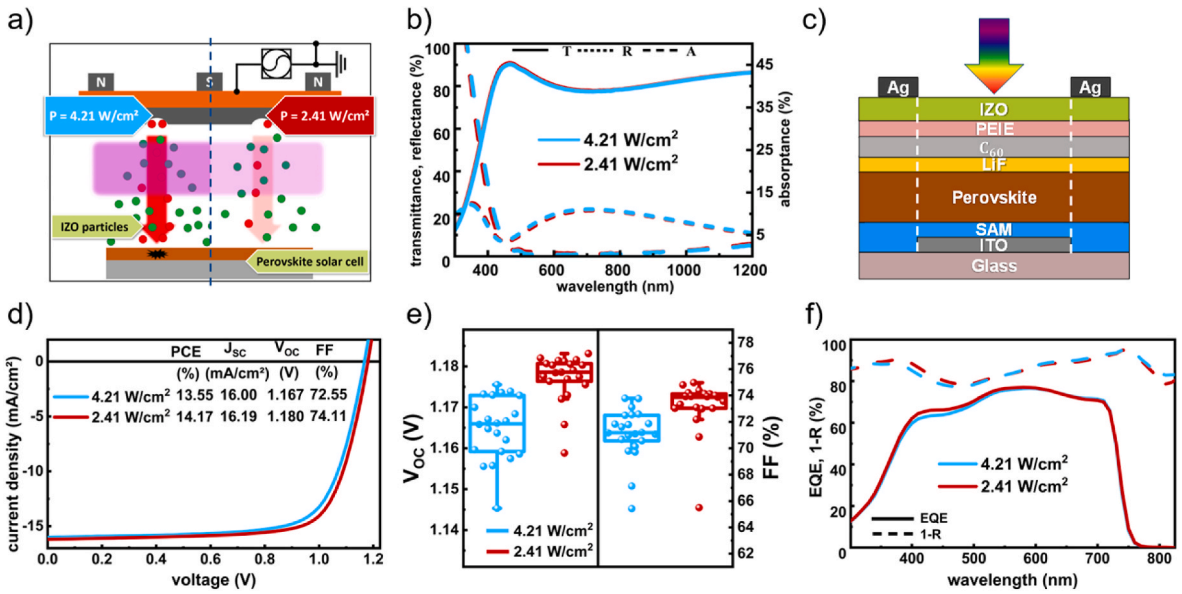

Fig. 1. (a) Schematic illustration and (b) transmittance, reflectance, and absorptance spectra of IZO films on glass of the 4.21 W/cm^2 and the 2.41 W/cm^2 RF sputter process. (c) Schematic illustration of the measured semitransparent single-junction solar cell stack and direction of illumination. (d) J-V characteristics and extracted values as inset, (e) boxplots for Voc and FF, and (f) EQE spectra of semitransparent perovskite single-junction solar cells with an IZO front-electrode sputtered at power densities of 4.21 W/cm^2 and 2.41 W/cm^2.

Table 1
Sputter process conditions for RF power densities of 4.21 W/cm^2 and 2.41 W/cm^2, optimized oxygen flow ratios for the respective processes, and resulting IZO thin film parameters.

Power density (W/cm^2)	Bias voltage (V)	Oxygen flow ratio (%)	Film thickness (nm)	Sheet resistance (Ω/sq)
4.21	200	0.25	100	44
2.41	140	0.1	100	41

perovskite absorber with a bandgap of 1.68 eV (value obtained from Rühle 2016 [26]). The detailed balance limit describes a theoretical solar cell in the radiative limit, where the only recombination processes are radiative originating from black body emission of the absorber film that depends on the absorber band gap and temperature [27]. The different loss contributions to the resulting device FFs are displayed in Fig. 2c.

A device's ideality factor usually exhibits a value between $n_{id} = 1$ and $n_{id} = 2$. While $n_{id} = 1$ describes solely radiative recombination processes, $n_{id} = 2$ describes a domination of non-radiative recombination (trap-assisted recombination) processes [28]. According to our measurements (see Fig. 2a), a higher RF sputter power IZO deposition leads to a higher ideality factor than a lower RF sputter power deposition – 1.50 for the 4.21 W/cm^2 process compared to 1.42 for the 2.41 W/cm^2 process. This suggests that the increase of V_{OC} and FF for reduced RF sputter power can be attributed to a reduction of trap-assisted recombination. The pseudo J-V curve and the FF loss contribution in Fig. 2b and c reveal that transport losses mainly contribute to the FF losses, being 0.86% absolute lower using reduced RF sputter power. The difference cannot be explained by the slightly different sheet resistances of the IZO electrode. At low light intensities, the TCO series resistance influence on the device FF becomes less significant [22]. Consequently, the individual FFs would converge at lower light intensities. However, we measured a FF of 75.85% for the 2.41 W/cm^2 and a FF of 74.20% for the 4.21 W/cm^2 process solar cell, leading to a difference of 1.65% at a light intensity of 0.1 suns (10%). This value is not lower than the difference in device FF at 1 sun (100%), which is 1.56%. We, therefore, conclude that the difference in transport losses likely originates from an increased contact resistance between the IZO electrode and the ETL. Oxidation of the ETL can cause such an increased contact resistance [29, 30]. Particularly physisorbed oxygen on C_{60} can significantly decrease electron transport [31]. The 4.21 W/cm^2 process has a higher additional oxygen content of 0.25%, while the 2.41 W/cm^2 process has only 0.1% oxygen mixed in. But we also consider damage to the ETL by sputtering as a probable explanation for the reduction in interfacial conductivity.

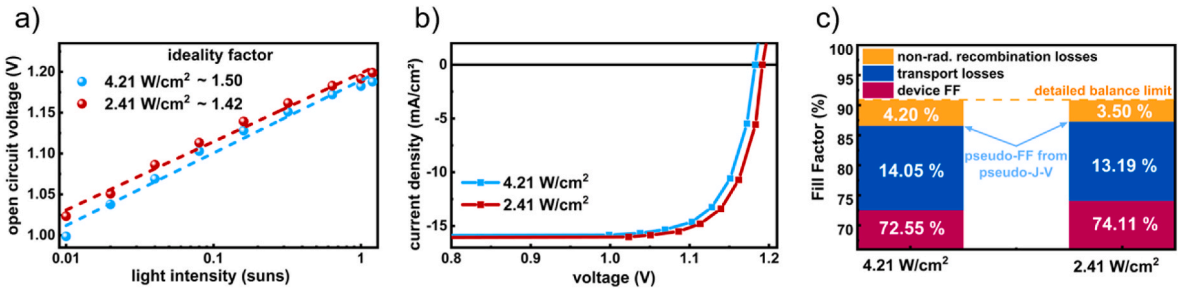

Fig. 2. (a) Light intensity-dependent V_{OC} and approximated ideality factor for single-junction devices with IZO front-electrodes sputtered at power densities of 4.21 W/cm^2 and 2.41 W/cm^2. (b) Pseudo J-V curves of the same cells were obtained by plotting the light intensity-dependent values of J_{SC} over V_{OC}. (c) FF losses were calculated by comparing the actual device FF and the pFF from the pseudo J-V curves to the detailed balance limit, considering the band gap of the perovskite absorber.

The difference in FF between the 4.21 W/cm^2 and the 2.41 W/cm^2 IZO deposition processes can furthermore be explained by the different contributions of non-radiative recombination losses, which reduce the FF by 4.20% in the case of the 4.21 W/cm^2 RF sputter power process and 3.50% in case of the 2.41 W/cm^2 RF sputter power process. In conclusion, we could correlate the impact of sputter damage on semi-transparent perovskite single-junction solar cells with transport losses and non-radiative recombination losses and increase the solar cell performance by reducing the RF sputter power.

We also want to investigate whether we can implement the soft IZO deposition on tin oxide (SnO_2) buffer layer-free monolithic two-terminal tandem devices, thereby reducing parasitic optical losses. Prior to the experiment, we performed optical simulations of the respective tandem device stacks in order to understand the impact of omitting the 20 nm thick SnO_2 buffer layer on the optical performance. For the simulation, the source of the layers optical data and the thicknesses are listed in Table S2. The simulation is done with GenPro4 [19]. For the simulation, the backside texture of the silicon sub-cell was taken into account, while all other layers were assumed to be optically flat (similar to Ref. [32]). We show the simulated EQE and the simulated contribution of the sub-cells currents in Fig. 3a, and the current losses to the total current density in Fig. 3b. The calculated short circuit current densities from the absorption profiles of the different sub-cell absorbers are unaffected by collection losses and hence represent idealized cases. The most significant gain in current density appears to be in the perovskite sub-cell, where the current density can be increased by 0.4 mA/cm^2, from 19.4 mA/cm^2 to 19.8 mA/cm^2, by omitting the SnO_2 buffer layer. This can mainly be attributed to the reduced parasitic absorption of 0.4 mA/cm^2, from 4.7 mA/cm^2 to 4.3 mA/cm^2, due to an extinction coefficient of SnO_2 unequal to zero in the relevant spectral range of perovskite absorption between 300 nm and 750 nm (see Fig. S5). The current density in the silicon sub-cell was also increased, from 19.4 mA/cm^2 to 19.6 mA/cm^2, while the reflection losses were likewise decreased from 2.9 mA/cm^2 to 2.8 mA/cm^2 by omitting the SnO_2 buffer. The sum of both sub-cell currents was increased from 38.8 mA/cm^2 to 39.4 mA/cm^2, attributing an overall 0.6 mA/cm^2 current density loss to the 20 nm thick SnO_2 buffer layer, which is an excellent motivation for omitting the SnO_2 buffer by implementing a directly deposited soft sputter-deposited IZO front electrode.

Finally, we tested the soft sputter-deposited IZO electrode on two-terminal tandem devices with and without the SnO_2 buffer layer. Here, we do not show results of two-terminal tandem devices with IZO electrodes sputtered at an RF power density of 4.21 W/cm^2 as the impact of sputter damage was already discussed above. Both designs presented in the following received a soft sputter-deposited IZO electrode (RF power density was set to 2.41 W/cm^2). We aim to point out that by implementing a soft IZO sputter deposition, a protective SnO_2 buffer layer is no longer required for high efficiency monolithic tandem solar cells. We measured the J-V curves and EQE spectra to validate the assumption that we can gain current by reducing parasitic optical losses without deteriorating other solar cell parameters by sputter damage. The results are given in Fig. 4. The tandem devices used for the comparison are identical, except for the layer between C_{60} and IZO. The tandem device labeled as "with SnO_2" was manufactured with a thermal atomic layer (ALD) deposited SnO_2 buffer layer in-between the C_{60} and the IZO. In contrast, for the tandem device labeled "w/o SnO_2", PEIE replaces the SnO_2. This tandem top cell has an equivalent design to the above-discussed semitransparent single junction solar cells. In this context, we neither acknowledge nor dismiss any buffer layer properties of the PEIE layer, which is thought to be about 2 nm thick [33]. A schematic representation of the tandem devices can be found in Fig. S6. The power conversion efficiency (PCE) of the tandem device with a buffer was 24.84%, and the device without a buffer reached a PCE of 25.44%. The higher PCE of the device without buffer can mainly be attributed to a higher device current density and FF, which were 0.52 mA/cm^2 and 0.85% higher for the SnO_2-free device. We attribute the increase in current density mainly to the increased silicon sub-cell current. However, contrary to previous observations (not shown here) for single-junction devices, a gain in V_{OC} was not found by replacing the SnO_2 with PEIE. We understand that the ALD deposition induces some degree of degradation to the perovskite which is reflected in a V_{OC} reduction. The EQE measurements and loss analysis given in Fig. 4b and c reveal that the current density of the silicon sub-cell limited the overall current density of the tandem devices. Both sub-cell short circuit current densities were increased by replacing SnO_2 with PEIE.

The spectral losses of both simulation (see Fig. 3a) and experiment (see Fig. 4b) reveal that for wavelengths between 300 and 600 nm, the experimental data agree well with the simulative prediction. We expect to see the benefits of omitting the parasitic absorbing SnO_2 buffer layer in this range. As shown in Table S3 in the supplementary section, corresponding with the parasitic absorption in the SnO_2 layer, mainly the parasitic absorption is reduced for wavelengths between 300 and 600 nm. For this region, the simulation predicts a reduction of the parasitic absorption of 0.27 mA/cm^2. In the experiment, the parasitic absorption was reduced by 0.22 mA/cm^2, which is in good agreement with the simulation. This results in a higher current in the perovskite of roughly 0.2 mA/cm^2 in both the simulation and the experiment for this wavelength range. Surprisingly, a significant difference in current density was observed for wavelength regions between 700 and 1200 nm. Here, an overall high reflection is measured for the cell with a SnO_2 buffer layer that, combined with relatively high EQE values, leads to reduced parasitic absorption losses in this wavelength regime. We speculate that this is related to thickness variations of the top-cell layers, the thin films in the recombination contact, or the electron-selective layers of the bottom cell. As a result, the overall reflection and parasitic absorption, as presented by the current loss analysis in Fig. 4c, taking a weighting and integration with the AM 1.5G spectrum into account, deviates slightly from the simulative current loss analysis in Fig. 3b. Nonetheless, we

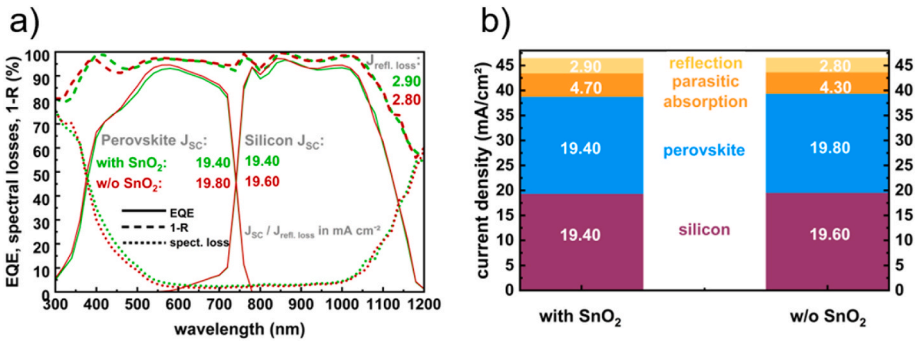

Fig. 3. (a) Optical simulations of perovskite/silicon tandem devices with and without a 20 nm thick SnO_2 buffer layer using GenPro4 including the spectral losses defined as difference between 1-R and the sum of the EQE spectra. (b) From the simulation derived current densities of each sub-cell and current density losses due to reflection and parasitic absorption. (For interpretation of the references to colour in this figure legend, the reader is referred to the Web version of this article.)

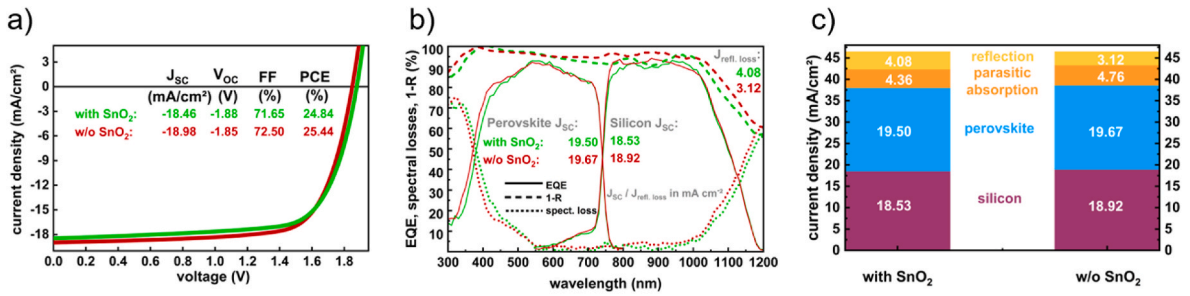

Fig. 4. (a) Comparison of the fabricated tandem J-V characteristic after spectral matching, with and without a 20 nm thick SnO_2 buffer layer. (b) Tandem EQE and 1-R spectra of the same tandem devices including the spectral losses defined as difference between 1-R and the sum of the EQE spectra. (c) Current density and current density losses analysis, based on the EQE and the 1-R measurements of the same devices.

want to stress that the optical advantage predicted by the simulation by omitting the SnO_2 buffer layer on the parasitic absorption in the perovskite top cell was experimentally reproduced.

These results show that a SnO_2 buffer layer-free tandem device employing a soft sputtered IZO electrode can outperform its SnO_2 counterpart due to superior optical performance. This optimisation could boost the current world record efficiency of 29.8% [2] obtained by using a SnO_2 buffer layer device even further.

4. Conclusion

We demonstrated a method to reveal the impact of sputter damage on the perovskite solar cell performance by correlating sputter damage-induced losses with recombination dynamics in the device. We achieved this by performing light intensity-dependent J-V measurements. Furthermore, we demonstrated a clear correlation between the applied IZO top contact sputter deposition power density and the perovskite solar cell performance by directly sputtering on the sensitive electron charge transport layer without using a protective SnO_2 buffer layer. We reduced the sputter power density from 4.21 W/cm^2 to 2.41 W/cm^2, which resulted in a higher V_{OC} for single-junction solar cells of ~13 mV and a higher FF of ~3%, overall improving the efficiency from 13.55 to 14.17%. These improvements correlate with reduced transport and trap-assisted non-radiative recombination losses. We simultaneously assured high-quality IZO films by optimizing the oxygen flow ratio of the IZO deposition processes prior to the solar cell integration to ensure similar IZO optoelectrical properties for both the 4.21 W/cm^2 and the 2.41 W/cm^2 sputter power processes. We then performed optical simulations for tandem devices with and without the SnO_2 buffer layer to show the expected optical improvements by omitting the SnO_2 buffer layer. We found that SnO_2 buffer layer-free tandem devices are less subjected to parasitic absorption losses and exhibit an overall 0.6 mA/cm^2 higher current density in sum. Finally, we integrated our sputter damage optimized IZO front electrode in an actual tandem device without a protective SnO_2 buffer layer and compared it with a conventional tandem device with a SnO_2 buffer layer. In doing so, an impressive gain of 0.52 mA/cm^2 current density was achieved in the final tandem device. Moreover, the fill factor was also 0.85% (absolute) higher for the SnO_2-free device. We believe that our approach will help to industrialize and optimize the optical performance of these fascinating tandem solar cells further.

CRediT authorship contribution statement

Marlene Härtel: Writing – review & editing, Writing – original draft, Visualization, Methodology, Investigation, Formal analysis, Data curation, Conceptualization. **Bor Li:** Writing – review & editing, Investigation, Formal analysis. **Silvia Mariotti:** Writing – review & editing, Formal analysis. **Philipp Wagner:** Resources, Formal analysis. **Florian Ruske:** Writing – review & editing, Investigation, Formal analysis. **Steve Albrecht:** Writing – review & editing, Supervision, Project administration, Funding acquisition. **Bernd Szyszka:** Writing – review & editing, Supervision, Project administration, Funding acquisition.

Declaration of competing interest

The authors declare that they have no known competing financial interests or personal relationships that could have appeared to influence the work reported in this paper.

Data availability

Data will be made available on request.

Acknowledgments

This work was funded by the German Federal Ministry for Education and Research (BMBF) for funding of the Young Investigator Group Perovskite Tandem Solar Cells within the program “Materialforschung für die Energiewende” (grant no. 03SF0540), the German Federal Ministry for Economic Affairs and Energy (BMWi) (“PersiST”, grant no. 0324037C), the Helmholtz Association through the HySPRINT innovation lab project. The authors would like to thank Dr. Philipp Tockhorn and Dr. Klaus Jäger from Helmholtz-Zentrum Berlin (HZB) for support with the optical simulation with GenPro4. The authors also acknowledge the support of scientific knowledge provided by Dr. Lars Korte from HZB. The authors acknowledge help in technical assistance with the sputtering tools by Mona Wittig, Thomas Luβky, and Martin Muske, and in perovskite lab assistance by Monika Gabernig, Carola Ferber, and Hagen Heinz from HZB.

Appendix A. Supplementary data

Supplementary data to this article can be found online at https://doi.org/10.1016/j.solmat.2023.112180.

References

[1] M. Jošt, L. Kegelmann, L. Korte, S. Albrecht, Monolithic perovskite tandem solar cells: a review of the present status and advanced characterization methods toward 30% efficiency, Adv. Energy Mater. (2020), https://doi.org/10.1002/aenm.201904102.
[2] National Renewable Energy Laboratory, Best Research-Cell Efficiency Chart, 2022. https://www.nrel.gov/pv/cell-efficiency.html. (Accessed 4 June 2022).
[3] M. Morales-Masis, S. De Wolf, R. Woods-Robinson, J.W. Ager, C. Ballif, Transparent Electrodes for Efficient Optoelectronics, 2017, https://doi.org/10.1002/aelm.201600529.
[4] J. Werner, G. Dubuis, A. Walter, P. Löper, S.J. Moon, S. Nicolay, M. Morales-Masis, S. De Wolf, B. Niesen, C. Ballif, Sputtered Rear Electrode with Broadband Transparency for Perovskite Solar Cells, Elsevier, 2015, https://doi.org/10.1016/j.solmat.2015.06.024.
[5] K.A. Bush, C.D. Bailie, Y. Chen, A.R. Bowring, W. Wang, W. Ma, T. Leijtens, F. Moghadam, M.D. McGehee, Thermal and environmental stability of semi-transparent perovskite solar cells for tandems enabled by a solution-processed

nanoparticle buffer layer and sputtered ITO electrode, Adv. Mater. 28 (2016) 3937–3943, https://doi.org/10.1002/adma.201505279.
[6] H. Scherg-Kurmes, A. Hafez, M. Siemers, A. Pflug, R. Schlatmann, B. Rech, B. Szyszka, Improvement of the homogeneity of high mobility In2O3:H films by sputtering through a mesh electrode studied by Monte Carlo simulation and thin film analysis, Phys. Status Solidi Appl. Mater. Sci. 213 (2016) 2310–2316, https://doi.org/10.1002/pssa.201532819.
[7] T. Wahl, J. Hanisch, S. Meier, M. Schultes, E. Ahlswede, Sputtered indium zinc oxide rear electrodes for inverted semitransparent perovskite solar cells without using a protective buffer layer, Org. Electron. 54 (2018) 48–53, https://doi.org/10.1016/j.orgel.2017.12.020.
[8] K. Tominaga, M. Chong, Y. Shintani, Energetic particles in the sputtering of an indium–tin oxide target, J. Vac. Sci. Technol. A Vacuum, Surfaces, Film. 12 (1994) 1435–1438, https://doi.org/10.1116/1.579333.
[9] E. Aydin, C. Altinkaya, Y. Smirnov, M.A. Yaqin, K.P.S. Zanoni, A. Paliwal, Y. Firdaus, T.G. Allen, T.D. Anthopoulos, H.J. Bolink, M. Morales-Masis, S. De Wolf, Sputtered transparent electrodes for optoelectronic devices: induced damage and mitigation strategies, Matter 4 (2021) 3549–3584, https://doi.org/10.1016/j.matt.2021.09.021.
[10] B. Demaurex, S. De Wolf, A. Descoeudres, Z. Charles Holman, C. Ballif, Damage at hydrogenated amorphous/crystalline silicon interfaces by indium tin oxide overlayer sputtering, Appl. Phys. Lett. 101 (2012) 1–5, https://doi.org/10.1063/1.4764529.
[11] K. Liu, B. Chen, Z.J. Yu, Y. Wu, Z. Huang, X. Jia, C. Li, D. Spronk, Z. Wang, Z. Wang, S. Qu, Z.C. Holman, J. Huang, Reducing sputter induced stress and damage for efficient perovskite/silicon tandem solar cells, J. Mater. Chem. (2022) 1343–1349, https://doi.org/10.1039/D1TA09143C.
[12] W. Tress, O. Inganäs, Simple experimental test to distinguish extraction and injection barriers at the electrodes of (organic) solar cells with S-shaped current-voltage characteristics, Sol. Energy Mater. Sol. Cells 117 (2013) 599–603, https://doi.org/10.1016/j.solmat.2013.07.014.
[13] H. Kanda, A. Uzum, A.K. Baranwal, T.A.N. Peiris, T. Umeyama, H. Imahori, H. Segawa, T. Miyasaka, S. Ito, Analysis of sputtering damage on I-V curves for perovskite solar cells and simulation with reversed diode model, J. Phys. Chem. C 120 (2016) 28441–28447, https://doi.org/10.1021/acs.jpcc.6b09219.
[14] J. Jia, Y. Torigoshi, Y. Shigesato, In situ analyses on negative ions in the indium-gallium-zinc oxide sputtering process, Appl. Phys. Lett. 103 (2013), 013501, https://doi.org/10.1063/1.4812668.
[15] S. Mariotti, K. Jäger, M. Diederich, M.S. Härtel, B. Li, K. Sveinbjörnsson, S. Kajari-schröder, R. Peibst, S. Albrecht, L. Korte, T. Wietler, Monolithic Perovskite/Silicon Tandem Solar Cells Fabricated Using Industrial P-type Polycrystalline Silicon on Oxide/Passivated Emitter and Rear Cell Silicon Bottom Cell Technology, 2022, 2101066, https://doi.org/10.1002/solr.202101066.
[16] A. Cruz, D. Erfurt, P. Wagner, A.B. Morales-vilches, F. Ruske, R. Schlatmann, B. Stannowski, Optoelectrical analysis of TCO+Silicon oxide double layers at the front and rear side of silicon heterojunction solar cells, Sol. Energy Mater. Sol. Cells 236 (2022), 111493, https://doi.org/10.1016/j.solmat.2021.111493.
[17] A. Al-Ashouri, E. Köhnen, B. Li, A. Magomedov, H. Hempel, P. Caprioglio, J. A. Márquez, A.B.M. Vilches, E. Kasparavicius, J.A. Smith, N. Phung, D. Menzel, M. Grischek, L. Kegelmann, D. Skroblin, C. Gollwitzer, T. Malinauskas, M. Jošt, G. Matič, B. Rech, R. Schlatmann, M. Topič, L. Korte, A. Abate, B. Stannowski, D. Neher, M. Stolterfoht, T. Unold, V. Getautis, S. Albrecht, Monolithic perovskite/silicon tandem solar cell with >29% efficiency by enhanced hole extraction, Science 80 (370) (2020) 1300–1309, https://doi.org/10.1126/science.abd4016.
[18] A. Pflug, V. Sittinger, F. Ruske, B. Szyszka, G. Dittmar, Optical characterization of aluminum-doped zinc oxide films by advanced dispersion theories, Thin Solid Films 455–456 (2004) 201–206, https://doi.org/10.1016/J.TSF.2004.01.006.
[19] R. Santbergen, T. Meguro, T. Suezaki, G. Koizumi, K. Yamamoto, M. Zeman, GenPro4 optical model for solar cell simulation and its application to multijunction solar cells, IEEE J. Photovoltaics 7 (2017) 919–926, https://doi.org/10.1109/JPHOTOV.2017.2669640.
[20] A.J. Leenheer, J.D. Perkins, M.F.A.M. Van Hest, J.J. Berry, R.P. O'Hayre, D. S. Ginley, General mobility and carrier concentration relationship in transparent amorphous indium zinc oxide films, Phys. Rev. B Condens. Matter 77 (2008) 1–5, https://doi.org/10.1103/PhysRevB.77.115215.
[21] M. Morales-Masis, S. Martin De Nicolas, J. Holovsky, S. De Wolf, C. Ballif, Low-temperature high-mobility amorphous IZO for silicon heterojunction solar cells, IEEE J. Photovoltaics 5 (2015) 1340–1347, https://doi.org/10.1109/JPHOTOV.2015.2450993.
[22] D. Glowienka, Y. Galagan, Light Intensity Analysis of Photovoltaic Parameters for Perovskite Solar Cells, 2022, 2105920, https://doi.org/10.1002/adma.202105920.
[23] S. Solak, A.G. Ricciardulli, T. Lenz, N.I. Craciun, P.W.M. Blom, G.A.H. Wetzelaer, Open-circuit Voltage Loss in Annealed P3HT : Perylene Diimide Bulk Heterojunction Solar Cells, 2017, pp. 1–5, https://doi.org/10.1063/1.4980842, 163301.
[24] S. Schiefer, B. Zimmermann, S.W. Glunz, Applicability of the Suns-V OC Method on Organic Solar Cells 4 (2014) 271–277.
[25] M. Stolterfoht, M. Grischek, P. Caprioglio, C.M. Wolff, E. Gutierrez-Partida, F. Peña-Camargo, D. Rothhardt, S. Zhang, M. Raoufi, J. Wolansky, M. Abdi-Jalebi, S.D. Stranks, S. Albrecht, T. Kirchartz, D. Neher, How to quantify the efficiency potential of neat perovskite films: perovskite semiconductors with an implied efficiency exceeding 28%, Adv. Mater. (2020), 2000080 https://doi.org/10.1002/adma.202000080.
[26] S. Rühle, Tabulated values of the Shockley–Queisser limit for single junction solar cells, Sol. Energy 130 (2016) 139–147, https://doi.org/10.1016/J.SOLENER.2016.02.015.
[27] W. Shockley, H.J. Queisser, Detailed balance limit of efficiency of p-n junction solar cells, J. Appl. Phys. 32 (1961) 510–519.
[28] P. Caprioglio, M. Stolterfoht, C.M. Wolff, T. Unold, B. Rech, S. Albrecht, D. Neher, On the relation between the open-circuit voltage and quasi-fermi level splitting in efficient perovskite solar cells, Adv. Energy Mater. 9 (2019), https://doi.org/10.1002/aenm.201901631.
[29] Y. Smirnov, P.A. Repecaud, L. Tutsch, I. Florea, K.P.S. Zanoni, A. Paliwal, H. J. Bolink, P.R. Cabarrocas, M. Bivour, M. Morales-Masis, Wafer-scale pulsed laser deposition of ITO for solar cells: reduced damage vs. interfacial resistance, Mater. Adv. 3 (2022) 3469–3478, https://doi.org/10.1039/D1MA01225H.
[30] C. Messmer, M. Bivour, C. Luderer, L. Tutsch, J. Schon, M. Hermle, Influence of interfacial oxides at TCO/doped Si thin film contacts on the charge carrier transport of passivating contacts, IEEE J. Photovoltaics 10 (2020) 343–350, https://doi.org/10.1109/JPHOTOV.2019.2957672.
[31] A. Tapponnier, I. Biaggio, P. Günter, Ultrapure C60 field-effect transistors and the effects of oxygen exposure, Appl. Phys. Lett. 86 (2005), 112114, https://doi.org/10.1063/1.1883327.
[32] E. Köhnen, P. Wagner, F. Lang, A. Cruz, B. Li, M. Roß, M. Jošt, A.B. Morales-Vilches, M. Topič, M. Stolterfoht, D. Neher, L. Korte, B. Rech, R. Schlatmann, B. Stannowski, S. Albrecht, 27.9% efficient monolithic perovskite/silicon tandem solar cells on industry compatible bottom cells, Sol. RRL 5 (2021) 1–8, https://doi.org/10.1002/solr.202100244.
[33] J.A. Raiford, C.C. Boyd, A.F. Palmstrom, E.J. Wolf, B.A. Fearon, J.J. Berry, M. D. McGehee, S.F. Bent, Enhanced nucleation of atomic layer deposited contacts improves operational stability of perovskite solar cells in air, Adv. Energy Mater. 9 (2019), 1902353, https://doi.org/10.1002/AENM.201902353.